Femtosecond Resolution of the Nonballistic Electron Energy Transport in Warm Dense Copper

A. Grolleau,[1,2,*] F. Dorchies,[2] N. Jourdain,[1,2] K. Ta Phuoc,[3] J. Gautier,[3] B. Mahieu,[3] P. Renaudin,[1] V. Recoules,[1] P. Martinez,[2] and L. Lecherbourg[1,3,†]

[1]*CEA, DAM, DIF, F-91297 Arpajon, France*

[2]*Université Bordeaux, CNRS, CEA, CELIA, UMR 5107, F-33400 Talence, France*

[3]*LOA, ENSTA, CNRS UMR 7639, Institut Polytechnique de Paris, F-91761 Palaiseau, France*

(Received 6 July 2021; revised 3 November 2021; accepted 14 December 2021; published 30 December 2021)

The ultrafast electron energy transport is investigated in laser-heated warm dense copper in a high flux regime ($2.5 \pm 0.7 \times 10^{13}$ W/cm^2 absorbed). The dynamics of the electron temperature is retrieved from femtosecond time-resolved x-ray absorption near-edge spectroscopy near the Cu $L3$ edge. A characteristic time of ~1 ps is observed for the increase in the average temperature in a 100 nm thick sample. Data are well reproduced by two-temperature hydrodynamic simulations, which support energy transport dominated by thermal conduction rather than ballistic electrons.

DOI: 10.1103/PhysRevLett.127.275901

The understanding of the electron energy transport is a fundamental issue in various fields of physics, ranging from femtosecond laser-driven phase transitions and processes [1–3], up to high energy density physics and laboratory astrophysics [4–6]. For instance, in ultrashort and moderate intensity laser interaction with matter, the speed and penetration of energy transport are key parameters for the tuning of in-depth matter modification. In the higher laser intensity regime, the knowledge of the thermal conductivity is of critical importance for the design of heating and compression of the nuclear capsule for inertial confinement fusion.

From the theoretical point of view, different regimes of laser-matter interaction lead to distinct treatments of the electron energy transport. In hot plasmas, the Spitzer-Harm theory is commonly used to determine the diffusive heat flux [7]. But this theory fails with strong temperature gradients, like the ones encountered in the high laser intensity regime. A limited flux factor has been proposed *ad hoc* to correct the heat flux and reproduce observations [8]. It has been adapted later thanks to more complex Fokker-Planck calculations [9] consistent with experiments [10,11], but it is still unable to highlight the involved physical processes. In condensed matter, at sufficiently low laser intensity and pulse duration, nonthermal electrons are first excited above the Fermi level within a small depth. They are then ballistically transported deeper, at approximately the Fermi velocity (~10^6 m/s). This simple model has been confirmed by measurements up to ~10^{10} W/cm^2 [12,13].

From the thermodynamic point of view, between these two situations, the matter is in the so-called warm dense matter (WDM) regime. Electron temperature is comparable to Fermi energy, and ions can be disordered but are still strongly coupled. This greatly complicates the prediction of physical properties required for fields directly linked to laser matter interaction, such as laser-induced damages [1–3], but also high-pressure science and planetology [5,14–16]. The theoretical description of matter in this regime is still a topical challenge (see, e.g., Ref. [17] and references therein). In particular, there is no theoretical consensus regarding the electron energy transport in the WDM regime, a process in competition with other ultrafast mechanisms such as electron-ion thermalization [18,19], phase transitions [20–22], or even hydrodynamic expansion [19]. Most femtosecond laser experimental studies assume ballistic transport to justify the ultrafast isochoric production of a homogeneous WDM sample over a thickness of the order of the electron mean free path [18,20–24]. This is supported by numerical works for laser intensity below 10^{13} W/cm^2 [25]. Far beyond that, diffusive transport is most often considered, and some thermal conductivity models have been proposed and even coupled to hydrodynamic codes (see Refs. [26–28]).

On the experimental side, the dynamics of electron transport has been studied mainly at low flux ($\lesssim 10^{10}$ W/cm^2), by measuring subtle changes (~10^{-5}) in the optical reflectivity of the sample rear side [12,13]. The observations supported a transport dominated by ballistic electrons. The need to renew the sample for a large number of laser shots severely limited the transposition of such accurate measurements beyond the damage threshold. More recently, Chen and co-workers proposed to use a chirped pulse to get single-shot time-resolved optical reflectivity on warm dense gold [29]. Unfortunately, besides the indirect relationship between electron temperature and optical reflectivity, the time resolution was not high enough (~500 fs) to access the transport dynamics through the 30 nm thick sample. Nevertheless, by comparing front-side and rear-side

measurements, they identified a flux limit Q_{NT} for ballistic electron transport. They proposed a simple but predictive model to establish its value, considering that the evacuated flux by ballistic electrons is limited by the energy they transport (Fermi energy E_F): $Q_{NT} = n_e E_F v_F$, where n_e and v_F are the electron density and Fermi velocity, respectively. Above this value, the authors suggested that diffusive transport should take over. But the experimental study of the electron transport dynamics is still to be performed in this regime.

In this Letter, we propose an original optical pump-x-ray probe experiment to investigate the electron energy transport with femtosecond resolution. For the first time, this method is applied to laser-heated warm dense copper, above the flux limit for the ballistic transport. Time-resolved x-ray absorption near-edge spectroscopy (XANES) spectra are measured near the $L3$ edge (~932 eV). They exhibit a preedge structure that has been proven to be a direct and in-depth diagnosis of the electron temperature T_e [18,19,30,31]. Two sample thicknesses of 30 and 100 nm are considered. A first set of data indicate that the absorbed laser energy is deposited and transported in a 30 nm layer in less than 100 fs. The following measurements show that the same amount of absorbed energy is transported through a 100 nm sample, with a characteristic time of ~1 ps, a much higher time than expected in the ballistic regime (~100 fs). These observations are in good agreement with hydrodynamic two-temperature simulations, favoring a diffusive transport of the electron energy.

The experiment was carried out at the LOA laboratory, on a dedicated setup which recently demonstrated the feasibility of femtosecond time-resolved XANES measurements with a betatron x-ray source [32]. The principle is sketched in Fig. 1. A 800 nm, 30 fs optical laser pulse ("pump") was focused on a copper sample, at a laser intensity that allows us to obtain an absorbed intensity exceeding the absorbed flux limit for nonthermal electrons Q_{NT}. The energy is deposited in the 12.7 nm skin depth

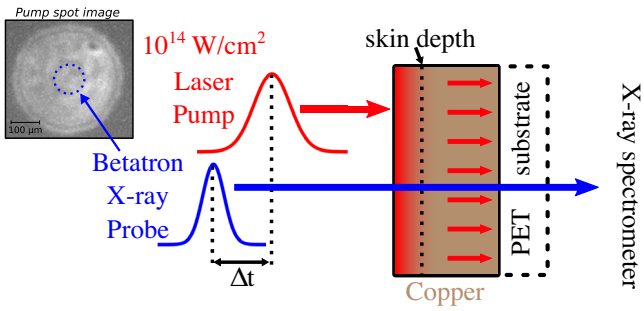

FIG. 1. Principle of the pump-probe experiment. A copper film is heated on one side by a femtosecond laser pulse and is probed by a femtosecond x-ray pulse which diagnoses the electron temperature and gives access to the time resolution of the electron energy transport from the energy reservoir (skin depth) to the depths of the sample.

[33], before being transported deeper. In copper, using $n_e = 8.49 \times 10^{22}$ cm^{-3}, $E_F = 7.04$ eV, and $v_F = 1.57 \times 10^8$ cm/s [34], $Q_{NT} = 1.5 \times 10^{13}$ W/cm^2 [29]. The electron mean free path (MFP) is 70 nm [35]. In such a pump-probe scheme, a synchronized femtosecond x-ray pulse ("probe") measured the evolution of the electron temperature in the depth of the sample.

Copper films have been deposited on a 1 μm thick Mylar™ substrate. Two thicknesses have been used. The first one was 30 ± 3 nm, close to the skin depth and thinner than the electron MFP, in which ultrafast homogeneous heating is expected. The second one was thicker, 100 ± 10 nm, in which the time-resolved T_e dynamics has been investigated during the electron energy transport. The pump laser fluence was 3.3 ± 0.9 J/cm^2, corresponding to an incident flux of $1.1 \pm 0.3 \times 10^{14}$ W/cm^2. The absorption has been measured at $23\% \pm 3\%$ in a dedicated experiment at CELIA facility, then cross-checked during the experiment at LOA laboratory. It leads to an absorbed flux $Q_{\mathrm{abs}} = 2.5 \pm 0.7 \times 10^{13}$ W/cm^2, so that $Q_{NT} = 0.6 \times Q_{\mathrm{abs}}$. The uncertainty on the laser flux was mainly due to spatial inhomogeneity, rather than to shot-to-shot fluctuations. The pump had a top-hat spatial profile on sample, with a diameter of 380 ± 10 μm. The angle of incidence was $2.2° \pm 0.2°$ from the normal.

The betatron x-ray pulse used as a probe is obtained from the relativistic interaction of a 30 fs, $\gtrsim 10^{19}$ W/cm^2 laser pulse with a supersonic gas jet (99% He / 1% N_2). It presents a broad synchrotronlike spectrum, very suitable for x-ray absorption spectroscopy [36]. A toroidal mirror, used at 2° grazing incidence, focused the x rays on sample at normal incidence, on a ~150 μm spot diameter. The x-ray spectra were recorded by a charge-coupled device (CCD) camera coupled with a rubidium acid phthalate cylindrical crystal in the Johann geometry [37]. The spectral calibration was measured from Cu $L3$ (932.5 eV) and $L2$ (952.5 eV) edges, and a ~1 eV spectral resolution was found. During the experiment, up to ~80 photons/eV/shot near the Cu $L3$ edge were measured on the CCD camera, corresponding to incident $\sim 4 \times 10^4$ photons/eV/shot on the sample.

The x-ray pulse duration is inferred from particle-in-cell simulations. A value of ~10 fs FWHM is calculated [32]. Considering both the pump duration (30 fs) and the geometric contribution (~20 fs between the two extreme parts of the probed diameter), the quadratic sum results in a theoretical time resolution of ~40 fs. The betatron duration has never been measured with such a short resolution, but previous published data have demonstrated overall time resolution better than 75 ± 25 fs with the same setup [32]. Measurements with the 30 nm copper sample corroborate this result (see below).

A XANES spectrum is deduced from the ratio between an x-ray spectrum transmitted through the sample by a reference spectrum without sample. The resulting experimental uncertainty is dominated by the photon counting

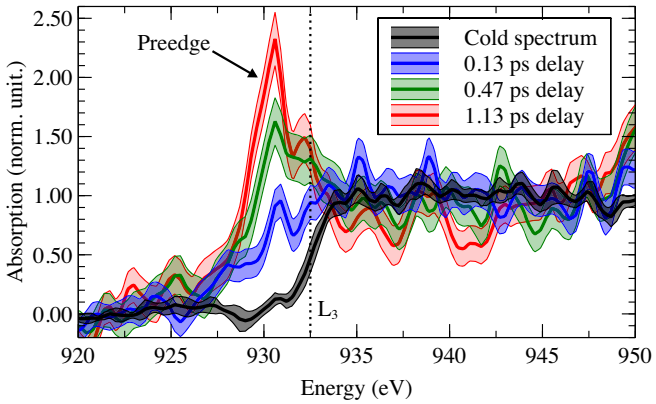

FIG. 2. Examples of XANES spectra recorded through 100 nm copper: at ambient ("cold") and at various delays after heating. The cold spectrum (black) is averaged over ∼1000 shots. The error resulting from the photon counting statistics is indicated by the colored areas.

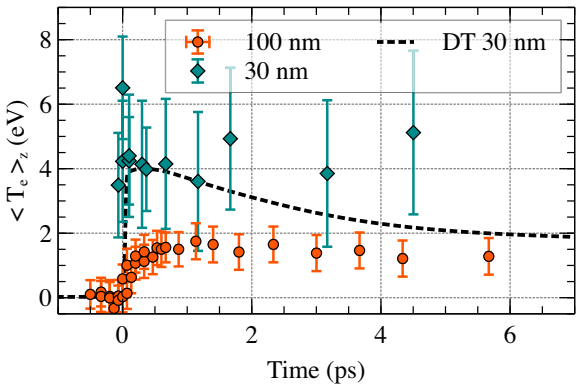

FIG. 3. Time evolution of the electron average temperature $\langle T_e \rangle_z$ measured in 30 nm (blue diamonds) and 100 nm samples (orange circles). Hydrodynamics TTM simulation for 30 nm diffusive transport (DT) is also represented (dotted black line), see Fig. 4 for details.

statistics on the detector. To improve this statistics, 100 shots per spectrum (and 100 more for the reference) have been accumulated, leading to ∼20 minutes to build each XANES spectrum. It was achievable thanks to the betatron shot-to-shot stability (8% rms) and a fully automated acquisition sequence. The relativistic interaction indirectly produces high energy photons which alter the signal on the detector. Appropriate shielding has been set up to reduce their number down to a reasonable amount. The few residual ones resulted in isolated hot spots which have been digitally removed.

Typical recorded XANES spectra are shown in Fig. 2 for several pump-probe delays in 100 nm copper. Near the copper $L3$ edge, a large preedge structure develops rapidly after heating and increases up to a delay of ∼1 ps. Previous work based on *ab initio* quantum molecular dynamics has demonstrated that the integral of this preedge structure is directly linked to the electron temperature T_e [19,31]. This work was used to infer an average value $\langle T_e \rangle_z$ of the electron temperature over the thickness coordinate z of the probed sample.

The deduced time evolution of $\langle T_e \rangle_z$ is reported in Fig. 3 for both 30 and 100 nm thick copper samples. The time origin is set to the maximum of the heating pulse (pump). Because the absorption level of 30 nm samples is about three times smaller than for the 100 nm ones, the error bars are higher. The data show that $\langle T_e \rangle_z$ increases up to 4.4 ± 1.9 eV in less than ∼100 fs, in the 30 nm sample. In 100 nm, it reaches 1.5 ± 0.5 eV in a longer time ∼1 ps. A decrease of $\langle T_e \rangle_z$ has already been measured on a longer time scale (∼10 ps), and is due to the electron-ion thermal equilibration [18,19,30].

Observations indicate ultrafast homogeneous heating in 30 nm, and incidentally demonstrate an effective time resolution better than 100 fs. A rough estimate of the expected temperature achieved can be made from the absorbed fluence $Q_{\mathrm{abs}} = C_e T_e d = 0.75 \pm 0.25$ J/cm^2, where $d = 30 \pm 3$ nm and $C_e = 6.6 \pm 1.9$ MJ/m^3/K is the electron heat capacity taken from [38] in the range of T_e considered. One finds $T_e = 3.3 \pm 1.5$ eV, in good agreement with the observation. Despite the large error bars, this shows that initially the energy deposit is essentially confined in copper rather than in the plastic behind, or in possible ejected electrons cloud [39–41].

The same estimation in the 100 nm sample leads to $T_e = 2.1 \pm 0.4$ eV, which is still in fairly good agreement with the measurements (here $C_e = 3.1 \pm 0.9$ MJ/m^3/K in the appropriate T_e range of 1.5 ± 0.5 eV [38]). The most important observation is that this maximal electron temperature is achieved only in ∼1 ps, which is significantly longer than the time resolution. This is also longer than expected with electron ballistic transport (∼100 fs). Considering a diffusive transport driven by the typical equation $C_e \partial T_e/\partial t = \vec{\nabla}(K_e \vec{\nabla} T_e)$, one can estimate a characteristic time $\Delta t \approx C_e l^2/K_e$. By setting l to the thickness of the energy reservoir (12.7 nm), and using the electron thermal conductivity $K_e \sim 4 \times 10^2$ W/m/K taken from [27,28], one finds $\Delta t \sim 1.2$ ps. This time (which further increases with higher values of l) is more consistent with the observations, which would indicate that the transport is in that case dominated by diffusion.

In order to explore more precisely the link between the inferred $\langle T_e \rangle_z(t)$ and the electron energy transport, one-dimensional hydrodynamic simulations were performed with the Lagrangian ESTHER code [42]. The two-temperature model (TTM) is consistently integrated, with T_e-dependent coefficients taken from Ref. [38] for the electron heat capacity C_e and the electron-ion coupling factor. The electron heat conductivity K_e is taken from Ref. [27]. The temporal profile of the energy deposit is set to the values of the absorbed pump pulse. The initial deposit in the skin depth is mimicked by a steep longitudinal

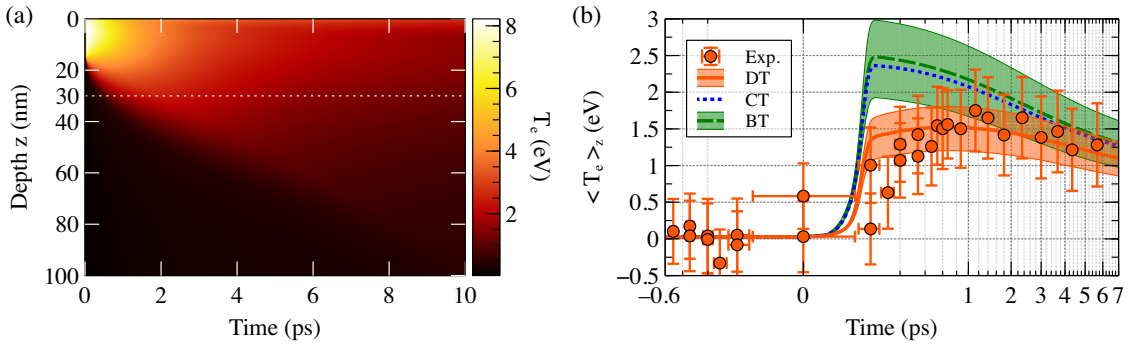

FIG. 4. (a) Simulated values of the electron temperature T_e (color scale) as a function of time and depth, in a 100 nm thick sample. The energy is deposited homogeneously in the electrons over a thickness of 15 nm, then transported deeper by diffusion. (b) Deduced values of $\langle T_e \rangle_z$ as a function of time (DT), compared both with data obtained by simulating ballistic transport (BT), a composite of 60% ballistic and 40% diffusive transport (CT), and with the 100 nm measurements (data of Fig. 3 close-up on the first 2.5 ps). The experimental uncertainty on the absorbed energy flux is reported in the colored areas surrounding calculations.

profile of 15 nm depth. Such a code is well suited to process diffusive transport. In order to simulate a faster ballistic transport, we considered an initial energy deposit on a thickness increased by the electron MFP.

The simulated electron temperature $T_e(t, z)$ is represented in Fig. 4(a), as a function of time t and depth z in the sample. At each time step, the average $\langle T_e \rangle_z$ is extracted over the whole Lagrangian positions of copper, weighted by the mass of numerical cells. Using the fact that T_e varies linearly with the preedge area in our temperature domain, we made sure that this value was equivalent to the $\langle T_e \rangle_z$ deduced from measurement. The results are computed for a 100% diffusive transport, a 100% ballistic transport and a composite of 60% ballistic and 40% diffusive transport to mimic the absorbed flux above the limit Q_{NT}. They are plotted in Fig. 4(b) and compared with measurements.

The first observation [Fig. 4(a)] is that the electron temperature is far from being homogeneous along 100 nm, when the experimental average temperature reaches its maximum (∼1 ps). If one focuses on the first 30 nm, the chain of calculation quickly leads to a maximum average electron temperature of 4.0 ± 0.8 eV (see Fig. 3). In this situation, the hypothesis of a ballistic transport does not significantly modify the dynamics of $\langle T_e \rangle_z$ (not presented). As shown in Fig. 4(b), this is no longer the case with a 100 nm sample. The experimental data are clearly not reproduced neither with ballistic transport nor with the composite transport calculation, whether one considers the maximum temperature reached or the corresponding time. On the other hand, the 100% diffusive calculation reproduces fairly well the experimental data. Even if the energy deposit is completed in 30 fs FWHM, the average electron temperature $\langle T_e \rangle_z$ continues to increase due to the strong T_e dependence of the electron heat capacity C_e. It reaches 1.5 ± 0.3 eV in 0.5–1 ps, in close agreement with the measurements. This confirms that the thermal diffusion is dominant in this regime above the flux limit Q_{NT}. That could be interpreted by a reduction of the electron range, as suggested by Li *et al.* [40] and Ogitsu *et al.* [43], who observed different behaviors of the front and rear sides of samples in similar heating conditions. It also corroborates previous measurements that show an increase of the electron collision rate with the electron temperature in the WDM regime [44].

The analysis based on the TTM assumes a thermalized electron population. This hypothesis might be highly questionable with laser fluence at the mJ/cm^2 level [45]. Nevertheless thermalization times shorter than 10 fs are expected in the high flux range investigated here ($Q_{\mathrm{abs}} = 0.75 \pm 0.25$ J/cm^2) [46,47] and support such assumptions. Other physical coefficients are directly involved in the diffusive electron transport equation $C_e \partial T_e/\partial t = \vec{\nabla}(K_e \vec{\nabla} T_e)$. The T_e-dependent electron heat capacity C_e taken from [38] essentially depends on the electron density of state which is not significantly modified from solid to warm dense copper [31]. It has been extensively tested and validated [18,19,30,31]. Different theoretical approaches can be used to calculate the thermal conductivity K_e (see, for instance, Refs. [27,28,48]). They seem to converge in the temperature range investigated in the present study but show significant differences either at high T_e ($\gtrsim$2 eV) or low T_e ($\lesssim$0.5 eV). Experimental results of the type reported here, with a better signal to noise ratio, should help to sort out these models.

As demonstrated here, the diffusion is slower than the ballistic transport. It can limit the heating homogeneity of a WDM idealized slab and compete with other dynamical processes such as electron-ion equilibration or phase transitions, confusing data interpretation at the femtosecond scale. Most of the previously published experimental work has considered ballistic transport. So far, to the best of our knowledge, the flux investigated was below the flux limit Q_{NT} proposed in [29] (see, for example, Refs. [18–23,30,49–53]). But this issue must be taken into account when studying cases with absorbed flux exceeding Q_{NT}. It might be crucial for processes expected at high

electron temperature, such as the bond hardening effects on the phase transition dynamics, predicted at $T_e \geq 3$ eV [54].

In conclusion, we have investigated the ultrafast electron energy transport dynamics in warm dense copper using femtosecond time-resolved XANES probing. Two sample thicknesses, respectively 30 nm and 100 nm, have been heated with 2.5×10^{13} W/cm^2 absorbed laser flux, in a regime above the flux limit for ballistic transport [29]. XANES spectroscopy allows the direct and in-depth measurement of the time evolution of the electron average temperature. In 30 nm copper, experimental data show a fast increase ($\lesssim$100 fs) up to ~4.5 eV, consistent with a homogeneous heating. In 100 nm, the same energy is absorbed, but more diluted in depth, leading to a maximum of ~1.5 eV. It is reached in ~1 ps, which is significantly longer than expected with a ballistic transport (~100 fs). Data are well reproduced with two-temperature hydrodynamics simulations, supporting an electron energy transport dominated by thermal conduction in such a high flux regime. Beyond the potential interest of this new type of experiment to test different heat conduction models, this study pinpoints the limits of ultrafast homogeneous heating of a warm dense matter idealized slab.

This work was supported by the French ANR agency under Grant No. ANR-21-CE30-0013. The authors thank J.-P. Goddet and A. Tafzi for the laser operation, and E. Blanc for the samples preparation.

*adrian.grolleau@cea.fr
†ludovic.lecherbourg@cea.fr

[1] Q. Feng, Y. N. Picard, H. Liu, S. M. Yalisove, G. Mourou, and T. M. Pollock, Scr. Mater. **53**, 511 (2005).
[2] E. G. Gamaly, Phys. Rep. **508**, 91 (2011).
[3] D. Tan, K. N. Sharafudeen, Y. Yue, and J. Qiu, Prog. Mater. Sci. **76**, 154 (2016).
[4] J. Nuckolls, L. Wood, A. Thiessen, and G. Zimmerman, Nature (London) **239**, 139 (1972).
[5] T. Guillot, Science **286**, 72 (1999).
[6] S. H. Glenzer *et al.*, Science **327**, 1228 (2010).
[7] L. Spitzer and R. Harm, Phys. Rev. **89**, 977 (1953).
[8] R. C. Malone, R. L. McCrory, and R. L. Morse, Phys. Rev. Lett. **34**, 721 (1975).
[9] J. P. Matte, T. W. Johnston, J. Delettrez, and R. L. McCrory, Phys. Rev. Lett. **53**, 1461 (1984).
[10] T. J. Goldsack, J. D. Kilkenny, B. J. MacGowan, P. F. Cunningham, C. L. S. Lewis, M. H. Key, and P. T. Rumsby, Phys. Fluids **25**, 1634 (1982).
[11] G. Schurtz, S. Gary, S. Hulin, C. Chenais-Popovics, J. C. Gauthier, F. Thais, J. Breil, F. Durut, J. L. Feugeas, P. H. Maire, P. Nicolai, O. Peyrusse, C. Reverdin, G. Soullie, V. Tikhonchuk, B. Villette, and C. Fourment, Phys. Rev. Lett. **98**, 095002 (2007).
[12] S. D. Brorson, J. G. Fujimoto, and E. P. Ippen, Phys. Rev. Lett. **59**, 1962 (1987).
[13] C. Suarez, W. E. Bron, and T. Juhasz, Phys. Rev. Lett. **75**, 4536 (1995).
[14] M. Ross, Nature (London) **292**, 435 (1981).
[15] D. Saumon, G. Chabrier, D. J. Wagner, and X. Xie, High Press. Res. **16**, 331 (2000).
[16] T. S. Duffy and R. F. Smith, Front. Earth Sci. **7**, 23 (2019).
[17] National Research Council, *Frontiers in High Energy Density Physics: The X-Games of Contemporary Science* (National Academic Press, Washington, D.C., 2003).
[18] B. I. Cho, K. Engelhorn, A. A. Correa, T. Ogitsu, C. P. Weber, H. J. Lee, J. Feng, P. A. Ni, Y. Ping, A. J. Nelson, D. Prendergast, R. W. Lee, R. W. Falcone, and P. A. Heimann, Phys. Rev. Lett. **106**, 167601 (2011).
[19] N. Jourdain, L. Lecherbourg, V. Recoules, P. Renaudin, and F. Dorchies, Phys. Rev. B **97**, 075148 (2018).
[20] R. Ernstorfer, M. Harb, C. T. Hebeisen, G. Sciaini, T. Dartigalongue, and R. J. D. Miller, Science **323**, 1033 (2009).
[21] M. Z. Mo *et al.*, Science **360**, 1451 (2018).
[22] N. Jourdain, L. Lecherbourg, V. Recoules, P. Renaudin, and F. Dorchies, Phys. Rev. Lett. **126**, 065001 (2021).
[23] K. Widmann, T. Ao, M. E. Foord, D. F. Price, A. D. Ellis, P. T. Springer, and A. Ng, Phys. Rev. Lett. **92**, 125002 (2004).
[24] A. Ng, T. Ao, F. Perrot, M. Dharma-Wardana, and M. Foord, Laser Part. Beams **23**, 527 (2005).
[25] A. Suslova and A. Hassanein, J. Appl. Phys. **124**, 065108 (2018).
[26] S. I. Anisimov, B. L. Kapeliovich, and T. L. Perel'man, Sov. Phys. JETP **39**, 375 (1974).
[27] S. I. Anisimov and B. Rethfeld, Proc. SPIE Int. Soc. Opt. Eng. **3093**, 192 (1997).
[28] K. P. Migdal, Y. V. Petrov, D. K. Il'nitsky, V. V. Zhakhovsky, N. A. Inogamov, K. V. Khishchenlo, D. V. Knyazev, and P. R. Levashov, Appl. Phys. A **122**, 408 (2016).
[29] Z. Chen, V. Sametoglu, Y. Y. Tsui, T. Ao, and A. Ng, Phys. Rev. Lett. **108**, 165001 (2012).
[30] B. I. Cho, T. Ogitsu, K. Engelhorn, A. A. Correa, Y. Ping, J. W. Lee, L. J. Bae, D. Prendergast, R. W. Falcone, and P. A. Heimann, Sci. Rep. **6**, 18843 (2016).
[31] N. Jourdain, V. Recoules, L. Lecherbourg, P. Renaudin, and F. Dorchies, Phys. Rev. B **101**, 125127 (2020).
[32] B. Mahieu, N. Jourdain, K. Ta Phuoc, F. Dorchies, J-P. Goddet, A. Lifschitz, P. Renaudin, and L. Lecherbourg, Nat. Commun. **9**, 3276 (2018).
[33] P. B. Johnson and R. W. Christy, Phys. Rev. B **6**, 4370 (1972).
[34] N. W. Ashcroft and N. D. Mermin, *Solid State Physics* (Harcourt College Publishers, New York, 1976).
[35] J. Hohlfeld, S. S. Wellershoff, J. Güdde, U. Conrad, V. Jähnke, and E. Matthias, Chem. Phys. **251**, 237 (2000).
[36] S. Corde, K. Ta Phuoc, G. Lambert, R. Fitour, V. Malka, A. Rousse, A. Beck, and E. Lefebvre, Rev. Mod. Phys. **85**, 1 (2013).
[37] H. H. Johann, Z. Phys. **69**, 185 (1931).
[38] Z. Lin, L. V. Zhigilei, and V. Celli, Phys. Rev. B **77**, 075133 (2008).
[39] Y. Ping, A. A. Correa, T. Ogitsu, E. Draeger, E. Schwegler, T. Ao, K. Widmann, D. F. Price, E. Lee, H. Tam, P. T. Springer, D. Hanson, I. Koslow, D. Prendergast, G. Collins, and A. Ng, High Energy Density Phys. **6**, 246 (2010).
[40] J. Li, J. Zhou, T. Ogitsu, Y. Ping, W. D. Ware, and J. Cao, High Energy Density Phys. **8**, 298 (2012).

[41] S. L. Daraszewicz, Y. Giret, N. Naruse, Y. Murooka, J. Yang, D. M. Duffy, A. L. Shluger, and K. Tanimura, Phys. Rev. B **88**, 184101 (2013).
[42] J.-P. Colombier, P. Combis, F. Bonneau, R. Le Harzic, and E. Audouard, Phys. Rev. B **71**, 165406 (2005).
[43] T. Ogitsu, Y. Ping, A. Correa, B. I. Cho, P. Heimann, E. Schwegler, J. Cao, and G. W. Collins, High Energy Density Phys. **8**, 303 (2012).
[44] C. Fourment, F. Deneuville, D. Descamps, F. Dorchies, S. Petit, O. Peyrusse, B. Holst, and V. Recoules, Phys. Rev. B **89**, 161110(R) (2014).
[45] M. Obergfell and J. Demsar, Phys. Rev. Lett. **124**, 037401 (2020).
[46] B. Y. Mueller and B. Rethfeld, Phys. Rev. B **87**, 035139 (2013).
[47] H. T. Chang, A. Guggenmos, S. K. Cushing, Y. Cui, N. U. Din, S. R. Acharya, I. J. Porter, U. Kleineberg, V. Turkowski, T. S. Rahman, D. M. Neumark, and S. R. Leone, Phys. Rev. B **103**, 064305 (2021).
[48] A. McKelvey *et al.*, Sci. Rep. **7**, 7015 (2017).
[49] T. Ao, Y. Ping, K. Widmann, D. F. Price, E. Lee, H. Tam, P. T. Springer, and A. Ng, Phys. Rev. Lett. **96**, 055001 (2006).
[50] Z. Chen, B. Holst, S. E. Kirkwood, V. Sametoglu, M. Reid, Y. Y. Tsui, V. Recoules, and A. Ng, Phys. Rev. Lett. **110**, 135001 (2013).
[51] Z. Chen, M. Mo, L. Soulard, V. Recoules, P. Hering, Y. Y. Tsui, S. H. Glenzer, and A. Ng, Phys. Rev. Lett. **121**, 075002 (2018).
[52] B. J. Siwick, J. R. Dwyer, R. E. Jordan, and R. J. D. Miller, Science **302**, 1382 (2003).
[53] F. Dorchies and V. Recoules, Phys. Rep. **657**, 1 (2016).
[54] V. Recoules, J. Clérouin, G. Zérah, P. M. Anglade, and S. Mazevet, Phys. Rev. Lett. **96**, 055503 (2006).